

Article

The Effect of Fiber Waviness on the Residual Stress State and Its Prediction by the Hole Drilling Method in Fiber Metal Laminates: A Global-Local Finite Element Analysis

Steffen Tinkloh ^{1,*}, Tao Wu ², Thomas Tröster ¹  and Thomas Niendorf ² 

¹ Chair of Automotive Lightweight Design, Faculty of Mechanical Engineering, Paderborn University, 33098 Paderborn, Germany; thomas.troester@uni-paderborn.de

² Institute of Materials Engineering, Metallic Materials, University of Kassel, 34125 Kassel, Germany; wu@uni-kassel.de (T.W.); niendorf@uni-kassel.de (T.N.)

* Correspondence: steffen.tinkloh@uni-paderborn.de

Abstract: In this paper, fiber waviness, as one of the most frequently occurring defects in fiber reinforced composites, is numerically investigated with regard to the formation of residual stresses in fiber metal laminates. Furthermore, the prediction of the residual stress state in the thickness direction by means of the simulated hole drilling method is studied. To this regard, a global-local finite element analysis based on the submodel technique is presented. The submodel technique essentially consists of two governing steps: In the first step, a global model is first utilized to calculate and analyze the residual stress distribution and deformation in the intrinsically joined hybrid structure. Effective cure-dependent thermo-elastic properties predicted by a numerical homogenization procedure were used to simulate the curing-process and analyze the residual stresses state. However, the dimension of the intrinsically manufactured hybrid plate is large compared to the diameter of the drilled hole (2 mm), so that a local model is necessary, which provides only a geometric partial portion of the global model. The local model takes the global stress state into account and is subsequently used to simulate the incremental hole drilling method with a refined mesh discretization. The production-related fiber waviness is modeled by an element-wise orientation approximating a sinus function. In order to validate the global-local modeling approach, a comparison between numerical results and experimental data from literature is presented. The comparison between global residual stress state (global model) and the simulated hole drilling method (local model) is used to assess the applicability and reliability of the hole drilling method in case of fiber waviness. It is found that an in-plane fiber waviness leads to a rather low variance of residual stresses over thickness. In case of an out-of-plane fiber waviness, oscillating residual stress fields occur over the entire thickness along the fiber direction. Moreover, the current limits of the incremental hole drilling method could be pointed out by the presented investigations. It is seen that the simulated results of the incremental hole drilling method are sensitive to waviness, even if the amplitude-wavelength-ratio is small. Without further adjustment of the calibration coefficients the oscillating stress and strain fields lead, in particular fiber waviness in thickness direction, to unreliable predictions. For the experimental application it can be concluded that the specimens have to be carefully examined with regard to fiber waviness.

Keywords: fiber metal laminate; residual stress; hole drilling method; fiber waviness; hole drilling simulation; finite element method



Citation: Tinkloh, S.; Wu, T.; Tröster, T.; Niendorf, T. The Effect of Fiber Waviness on the Residual Stress State and Its Prediction by the Hole Drilling Method in Fiber Metal Laminates: A Global-Local Finite Element Analysis. *Metals* **2021**, *11*, 156. <https://doi.org/10.3390/met11010156>

Received: 15 December 2020

Accepted: 11 January 2021

Published: 15 January 2021

Publisher's Note: MDPI stays neutral with regard to jurisdictional claims in published maps and institutional affiliations.



Copyright: © 2021 by the authors. Licensee MDPI, Basel, Switzerland. This article is an open access article distributed under the terms and conditions of the Creative Commons Attribution (CC BY) license (<https://creativecommons.org/licenses/by/4.0/>).

1. Introduction

Today an automotive body in white (BIW) is inspired by a multi material design. In addition to classical lightweight materials like aluminum and magnesium alloys, advanced high strength steels (AHSS) are increasingly used due to high strength, good formability and enhanced crash performance. However, lightweight potential of these material classes

is still limited due to high density, buckling problems related to reduced sheet thickness or relatively low Young's modulus. On the other hand, carbon fiber reinforced plastics (CFRP) offers superior lightweight characteristics and high energy absorption [1]. However, CFRP have not achieved an acceptance like metals, which can be related to their comparably high production cost [2]. Therefore, hybrid materials allow to combine metals and CFRP in a manner to offset the drawbacks of every single material and reach an optimum of mechanical properties and costs. The comparably expensive lightweight material is then only partially used for local reinforcement of mechanically highly stressed regions, such as b-pillars or roof beams [3]. In addition to the application of hybrid materials in the body of white concepts, fiber metal laminates (FML) are extensively used in aircraft structures, due to their excellent damage tolerance and high weight saving potential compared to solitaire materials [4].

The hybridization process of a metal and CFRP component can be established by several ways. Downstream processes, where the forming process of the CFRP components and the assembling with the metal part are achieved within two separate process steps, have been well established [5]. The actual bonding between the metal and CFRP part can be achieved by mechanical or adhesive bonding technologies [6]. On the other hand, a new process chain approach, referred to as "intrinsic hybridization", has been introduced in [5] as follows: "An intrinsic hybrid is an integral component for which the connection of the different materials is carried out by primarily shaping or forming the metallic or continuous fiber-reinforced component." Due to intrinsic hybridization, a subsequent joining process is not necessary anymore, as the resin system of the prepreg provides the connection between the metal and the CFRP. Therefore, the intrinsic hybridization offer the advantage that the process steps required for lightweight component production can be reduced in total, and time- and cost-efficient production of metal/CFRP hybrids can be achieved. However, the backbone of intrinsically joined laminates is the residual stress state in the components resulting from the difference in thermal expansion coefficient (CTE) of the fiber and metal after cooling down from molding temperature. According to [7], the residual stress state can be divided with regard to their origin into three categories: Starting from the micro-scale of the CFRP, residual stresses are induced due to the difference in thermal expansion of fiber and matrix, as well as chemical shrinkage during the polymerization of the epoxy resin. On the meso-scale, residual stresses are the result of the different orientation of adjacent laminates, leading to a transverse isotropy of thermal expansion due to its microscopic heterogeneity. Finally, inhomogeneous temperature fields and different cooling rates are responsible for residual stresses on the macroscopic or part level. Since residual stresses are inherently present in FMLs and influence the overall behavior, like spring-in-effects [8], durability and damage accumulation [9], it is an essential task to predict and take into account the residual stresses in the design process [7]. A holistic assessment of the residual stress state during the curing process needs an adequate representation of the complex constitutive behavior of the preimpregnated preforms, as well as a multiscale approach to account for the origin of residual stress on several length scales [10]. To this regard, advanced simulation techniques and constitutive models have been developed by several authors [11,12].

Nonetheless, reliable tools for determination of residual stresses are required for validating the numerical simulations. There are various approaches to measure residual stresses. The commonly used non-destructive X-ray diffraction cannot be applied to fiber reinforced plastics, since it is restricted to crystalline materials [13]. The same holds true for synchrotron and neutron diffraction techniques [13]. Nanoindentation is an alternative method for determining the residual stresses [14]. However, inconsistencies among the residual stress results obtained by different calculation models for different materials and different processing methods limit the application [15]. In [16] fiber Bragg grating sensors were used to measure residual strains for a systematic analysis and evaluation of residual stress states in fiber metal laminates. Nonetheless, the proposed method is limited in that way that only an averaged or effective strain can be determined. Especially for

unsymmetrical layups the applicability of the method is restricted, as non-homogeneous residual stresses prevailing in thickness direction cannot be predicted or measured. The semi-destructive incremental hole drilling method (HDM) is a promising approach for measuring in-depth residual stresses in thickness direction, which can be applied to metal, as well as to the CFRP component [17]. In order to determine the stress states by means of the HDM, a small hole is drilled incrementally. Commonly, a strain gauge with three rosettes is applied onto the surface of the sample, where the hole is incrementally drilled in the center of the strain gauges. With each drilling step, a relaxation takes place, as a new equilibrium state is adjusted. The relaxation is measured by the strain gauges and can be related with some formulas to the original residual stress state at the hole center [18]. In [13], the standardized hole drilling method was extended by means of an orthotropic material model, a customized drilling increment size of 20 μm , as well as a customized strain gauge with 8 rosettes. The authors have shown that the specific characteristics of CFRP were successfully addressed by the extended hole drilling method. Reliable measurement from the surface up to a depth of 800 μm was realized in the CFRP. The validation with numerical stress predictions postulates the reliability of the employed hole drilling method. For a further establishment of the HDM method in fiber reinforced plastic, it is of high importance to investigate the applicability of the incremental hole drilling method with regard to common defects. This is quite important, as defects like fiber waviness, especially within geometrically complex components, cannot be completely avoided.

In order to obtain a comprehensive understanding about the above stated problem, numerical simulation methods are well suited. Two principal approaches are available to simulate the drilling process that is performed as part of the incremental hole drilling method. The first one considers the explicit modeling of the dynamic drilling process. Information about damages and delamination around the borehole, as well as the borehole quality itself can be predicted by this approach [19,20]. Several material combinations like CFRP [21], glass fiber aluminum reinforced epoxy (GLARE) [22] or CFRP/titan hybrids [23] were numerically investigated by varying process parameters. The results of these investigations cannot be directly transferred to the hole drilling method used in the presented work, as different drilling speed, feed rate, diameter and geometry of drill bit influence the released strains and the evaluated residual stresses [24,25]. In addition, if improper drilling process parameters are utilized, the damage and delamination may be induced in the composite, which significantly affects the reliability of the prediction. Aamir et al. [26] provides a comprehensive study on the role of drilling parameters and composite properties on the drilling-induced damage in machined holes. Moreover, this review examines the drilling process parameters and adequate optimization techniques.

In the incremental hole drilling method investigated here, a hole diameter of 2 mm in conjunction with a drilling increment of 20 μm was adopted [13]. Accordingly, an element edge length of at least 20 μm along the thickness is required. The fiber diameter of the fiber-reinforced plastics studied here is about 5 μm to 7 μm . The commonly used damage and fracture models (see for example [27]) neglected the microscopic inhomogeneity, instead a homogeneous material is assumed. This implies the need of a sufficient scale separation [28]. This is no longer fulfilled for element edge lengths of 20 μm and fiber diameters of 7 μm . Thus, the application of the conventional damage models is no longer justified, so that the underlying microstructure would have to be explicitly resolved. However, the dimensions of hole diameter and strain gauge are still large as compared to the fiber diameter (see Figure 2), so the meshing would end up in several million elements, thus resulting in extremely high computational cost. Furthermore, the small element edge length negatively affects the stable time increment. Alternatively, the analysis of the hole drilling method can be extended to the microscopic level. However, for ensuring a reasonable computational cost, the dimensions of the model remain limited to the microscopic level. In summary, the investigations of machining processes are based either on the analysis

of homogeneous laminates neglecting the underlying microstructure [20–22,29], or on the microscopic analysis of representative samples of fiber-matrix structures [30].

The second principal approach to simulate the machining process is based on an implicit representation of the cutting operation. Instead of explicitly modeling the contact and interaction between drill and workpiece, the method is based on incrementally removing defined sets of elements using an element removal technique. Thermo-mechanical residual stresses induced by the drilling process itself are not taken into account by this approach. Despite the comparatively simple representation of the machining process, previous work on residual stress determination in fiber-reinforced composites [24,31], as well as metallic materials including plasticity effects [32], has shown a very well agreement with experimental results.

In general, the formation of flaws and defects can be related to the manufacturing process itself and furthermore to the geometric complexity of the component. As fiber waviness is one of the most common defects in fiber reinforced plastics, many researchers investigate the origin itself [33]. The origin of the formation of fiber waviness in carbon fiber reinforced plastics can be related to several mechanism. The mismatch between thermal expansion coefficients of tool plate and part was found to be the most critical mechanism for its development [34]. Fiber waviness is commonly classified as in-plane and out-of-plane, as well as uniform, graded and localized waviness, thus resulting in eight possible combinations of waviness [35]. In recent years, several approaches based on analytical and numerical models describing different kinds of fiber waviness, have been developed to study the effect on the mechanical performance of the fiber reinforced plastics and structures [33,36–38]. An analysis of representative volume elements (RVE) with a defined fiber waviness was performed in [39] to study the effect on microscopic thermal residual stress. It was found that the fiber waviness has a negligible impact on the internal stresses on the micro-scale, as there are only minor deviations compared to the straight fiber unit cell. An analytical model based on the classical laminate theory was developed in [40] to take into account the effect of an out-of-plane waviness with respect to the elastic moduli of composite laminates. By a systematic investigation of various parameters of wavy laminates, the authors reported a major effect on the lateral and transversal (through-thickness) Young's modulus, and shear modulus in the x - z plane. The wave amplitude to wavelength ratio, the maximum off-axis angle, the dimensions of the wavy region, the waviness pattern and the laminates lay-up were concluded as the most sensitive parameters, respectively.

Nonetheless, to the best of the author's knowledge, no work has been carried out to study the effect of a fiber waviness with respect to the residual stress state in metal/CFRP hybrids, as well as its determination by means of the incremental hole drilling method. The aim of this study was to investigate the effect of fiber waviness on the residual stress state in intrinsically manufactured metal/CFRP hybrids, as well as its prediction by means of the hole drilling method. For this purpose, a global-local finite element model is developed. First, a simulation of the manufacturing process is presented. With the presented approach, the overall (theoretical) residual stress state in the metal/CFRP hybrid can be predicted. On the basis of a numerical homogenization scheme the effective cure-dependent elasticity parameters, as well as the effective cure-dependent coefficient of thermal expansion and the chemical shrinkage coefficient for the CFRP, have been predicted. Varying the element-wise orientation, a fiber waviness is introduced and its effect on the residual stress state is discussed. Moreover, different amplitude-wavelength-ratios, as well as out-of-plane and in-plane waviness are studied. In a second step, the prediction capacity and reliability of the incremental hole drilling will be analyzed with respect to the previously introduced fiber waviness configurations. Using an element removal technique, the elements in the hole area are deleted from the model representing the hole drilling process. After each drilled increment, the relaxed strains around the hole under the strain gauge position are calculated. With the calibration coefficients presented in [13], a calculation of the residual stress state using the simulated hole drilling method is done. The theoretical residual

stress state calculated by the manufacturing simulation and the prediction by means of the simulated hole drilling method are compared. Finally, a comparison of the experimental data from [13] and the simulation model is presented.

2. Simulation of Residual Stress States in Metal/CFRP Hybrids and Its Prediction by the Simulated Hole Drilling Method

In the following section, a node-based submodel technique acting as a model reduction method is presented. The submodel technique essentially consists of two governing steps. The residual stress and deformation state is determined using the global model and then mapped to the local model, which represents only a selected geometric detail of the entire specimen. The local model is subsequently used to simulate the hole drilling method with a refined discretization. Finally, the residual stress states of the global model (theoretical residual stress state) can be compared with the residual stress state determined by the simulated hole drilling method. The comparison is used to assess the applicability of the hole drilling method in case of imperfections. In the following, the local and global model will be presented. The section closes with a validation of the approach.

2.1. Global-Local Finite Element Analysis

In [10], the authors presented a multiscale finite element model to simulate the intrinsic hybridization of a plane metal/CFRP composite. Effective cure-dependent properties predicted by a numerical homogenization procedure were used to simulate the curing-process and analyze the residual stresses of a metal/CFRP plate. The results were compared with experimental data obtained by the incremental hole drilling measurement, reported in [13]. The model was adopted to study the effect of fiber waviness on the residual stress evolution in the intrinsic manufacturing process and is briefly summarized in the following part. Further details on the homogenization procedure and the related process simulation can be found in [10].

A holistic assessment of the development of residual stresses during the curing process needs an adequate representation of the complex constitutive behavior of the preimpregnated preforms. On the basis of representative volume elements, effective cure-dependent material properties were determined in [10] based on a numerical homogenization strategy to consider the curing mechanism of the epoxy. The effective cure-dependent material properties were also adopted for the presented simulations. The entries of the effective transverse isotropic elasticity tensor are shown in Figure 1 as a function of degree of cure. In addition to homogenized stiffness, effective coefficients of thermal expansion (CTE) and chemical shrinkage (CCS) were also predicted. The degree of cure was calculated using the user subroutine USDFLD [41]. The transversal effective thermal expansion coefficient and the effective chemical shrinkage coefficient were specified for the CFRP laminate using the user subroutine UEXPAN. The elasticity parameters were stored as tabulated data depending on a field variable (degree of cure).

Nonetheless, it should be noted that the driving-force is the difference in thermal expansion coefficient of metal and CFRP and that the curing process itself has a minor influence on the overall deformation and stress state considering the selected process and material parameters. An uncoupled thermo-mechanical analysis was defined to simulate the intrinsic hybridization process. Due to the comparatively small dimensions of the investigated sample (see Figure 2), it is reasonable to assume a constant temperature field. According to the manufacturing process a constant curing temperature of 160 °C was defined for an interval of 400 s. Up to this point, the curing process is almost completed and the specimen is cooled down from molding temperature to ambient temperature (20 °C). Since rate-effects are not taken into account (e.g., viscoelasticity is not defined), cooling down is not defined as a time-dependent step. The described temperature-time profile is shown in Figure 3a and is prescribed over the entire section and time. The metallic component is assumed to behave isotropic elastic. The corresponding material parameters are listed in Table 1. The geometrical details of the investigated specimen are given in Figure 2. Displacement boundary conditions are applied due to the symmetry related to

the y - z plane. Applying an in-plane fiber waviness in the following sections, the symmetry with respect to the x - z plane is not valid any longer and is therefore neglected. The metallic, as well as CFRP component were modeled as a three-dimensional structure using reduced integrated continuum elements (C3D8R). For a sufficiently accurate stress distribution in thickness direction, the element length was chosen as approximately $0.3 \times 0.3 \times 0.125$ mm ($w \times h \times t$). The connection between the constituents is assumed to be rigid throughout and modeled using the tie-constraint functionality. The presented computations have been performed using the implicit finite element solver Abaqus/Standard.

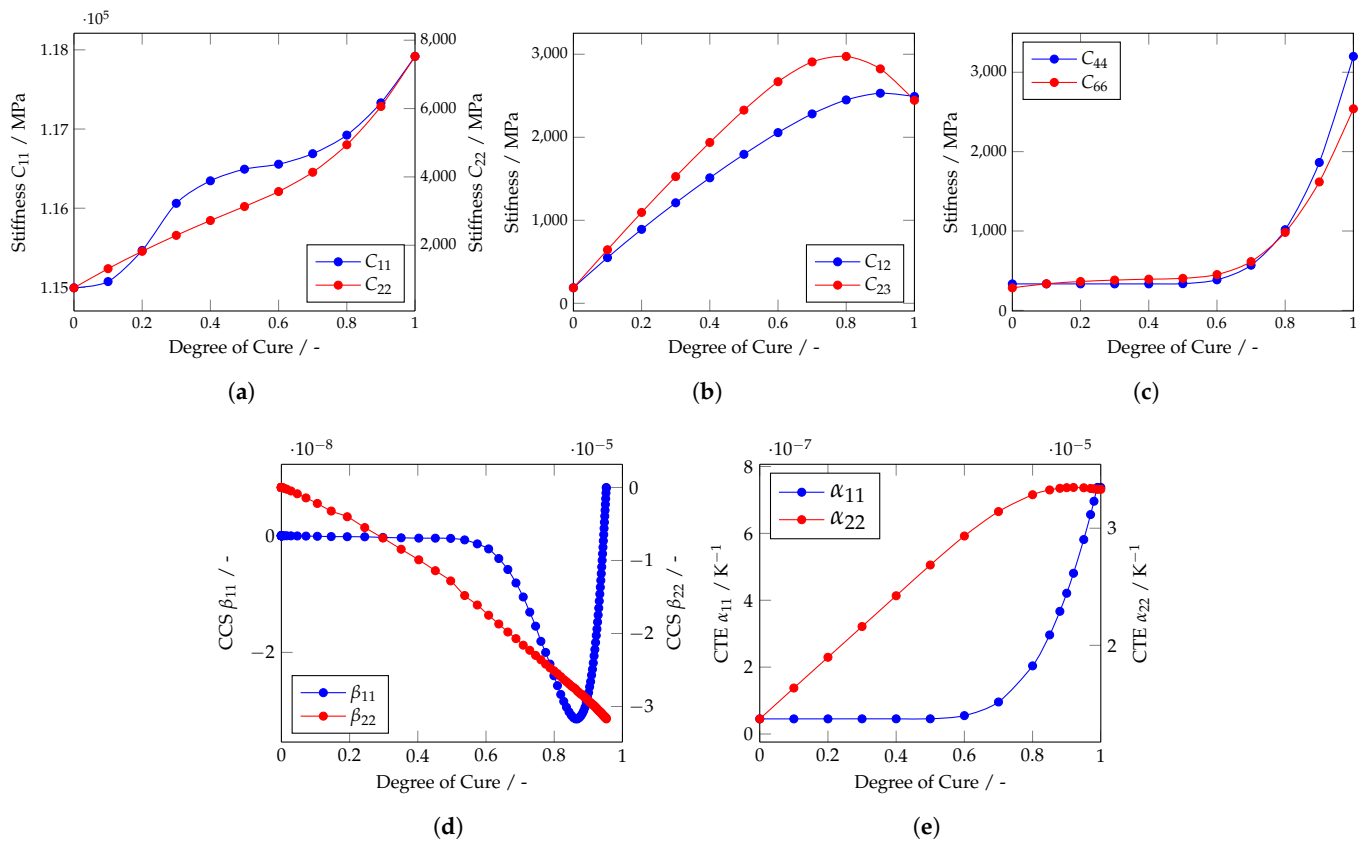


Figure 1. Evolution of the direct elastic coefficients as a function of the degree of cure (a–c). Due to the assumption of the transversal isotropy, the terms C_{22} and C_{33} are equal and C_{12} and C_{13} are equal. (d,e) Evolution of the effective transversal isotropic coefficient of chemical shrinkage (CCS) and coefficient of thermal expansion (CTE) as a function of degree of cure [10].

Table 1. Values of material parameters for the steel plate [10].

E	ν	α^{th}
210 GPa	0.29	1.2×10^{-5}

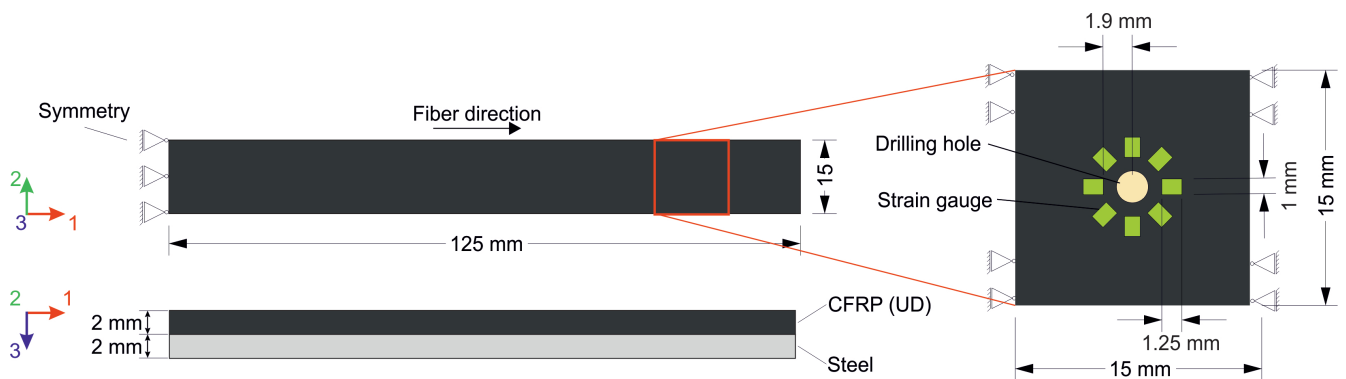


Figure 2. On the left side, the geometry and boundary conditions of the considered metal/CFRP hybrid are shown. Due to the symmetry within the 2–3 plane, the displacement is frozen. The derived submodel, as well as the arrangement of the drilled hole and the strain gauges, are shown on the right side.

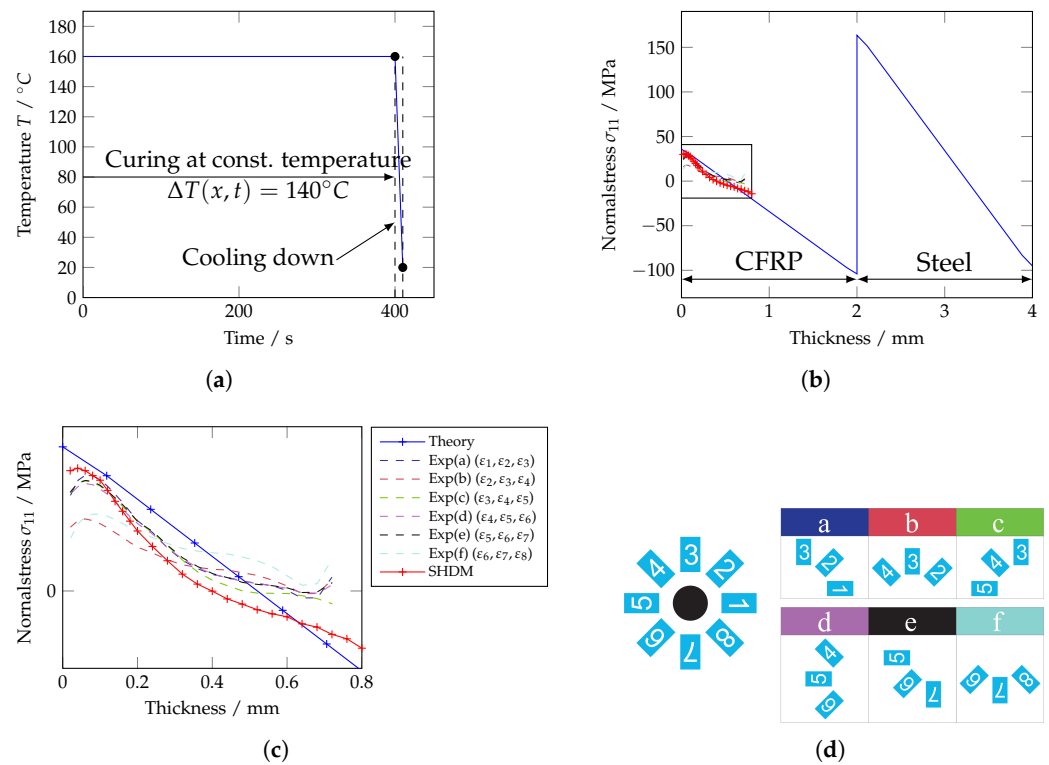


Figure 3. (a) Prescribed temperature-time profile $T(x, t)$ for the whole domain. (b) Corresponding residual stress state in thickness direction after completed curing and cooling down to ambient temperature. (c) Validation of the predicted residual stress state in thickness direction based on results obtained by the incremental hole drilling method. For the residual stress analysis using the hole drilling method six combinations of strain gauges were used. The strain gauge combinations are depicted in (d) [10]. In addition, the simulated hole drilling method (SHDM) is compared with experimental results in (c).

In order to simulate the hole drilling method, the local model that covers the drilling hole and the area of the applied strain gauges was defined as follows. Figure 2 depicts the geometric dimension of the model, as well as the position and size of the strain gauges around the drilling hole. The eight strain gauges are located on the surface of the CFRP. The geometry was set up using the partition tool available in Abaqus/CAE, so that the marked positions of the strain gauges could be meshed in a structured way. In addition, the hole with a diameter of 2 mm was defined in a similar way. The element edge length in these areas was refined and has an element size of approximately 40 μm

($w \times h$), whereas the element edge length of the remaining structure is about 150 μm . In the thickness direction an element edge length of 20 μm was utilized in accordance to the drilling increment size. The link between the local and global model is specified by boundary conditions accomplished with the submodel option. The boundary conditions are specified on the cut surfaces of the local model, so that the governing residual stresses and deformation are adequately defined. In a last step, the deformed geometry, as well as the stress distribution of the local model are imported once again using the import functionality in order to simulate the actual hole drilling process. The displacements on the cut surfaces are constrained accordingly.

An explicit simulation of the hole drilling process, e.g., explicit modeling of the contact between tool and work piece, is not feasible for the envisaged studies. In order to simulate the drilling process, an implicit representation is considered using the element deletion function. The functionality is called “model change” in Abaqus and is defined within the intersection module in Abaqus/CAE. Defined layers representing the drilled hole are removed incrementally. For a sufficient resolution of released strains, a drilling increment of 20 μm was adopted from the experimental study [13]. Viscoelasticity or –plasticity was not defined in the model, so in contrast to the experimental procedure, no relaxation had to be taken into account after each increment. The released strains are determined at the integration points of the elements, which are consistent with the geometric dimensions and the positions of the strain gauges. For the evaluation of the released strain the arithmetic mean of the elements, which defines a strain gauge, was used. With the formula given in [13], the released strains can be used to predict the residual stress state. Despite the comparatively simple representation of the machining process, previous work on residual stress determination in fiber-reinforced composites has shown a very good agreement with experimental results [31].

2.2. Comparison between Experimental Data and Numerical Modeling

In order to validate the global-local modeling approach, a validation with experimental data is presented finally. For this purpose, the results of the global model (referred to as Theory), as well as the results of the simulated hole drilling method (referred to as SHDM) obtained by the local model will be compared with data obtained by the experimental stress measurement through hole drilling method. The residual stresses were only measured on the CFRP side.

The principal procedure of the experimental hole drilling method is summarized as follows. For improving the reliability of the measurements a strain gauge with eight grids manufactured by Höttinger Baldwin Messtechnik (HBM, Darmstadt, Germany) was used in [13] for measuring the strain in the CFRP, and six combinations of strain gauge grids were employed. The combination of strain gauges is defined in Figure 3d. The strain gauge was connected to a quarter bridge with a feeding voltage of 1 V for the CFRP. A tool made of tungsten carbide (ref. H2.010, Gebr. Brasseler GmbH & Co. KG, Lemgo, Germany) was used for drilling. With respect to the general theory, a small drilling step size of 20 μm was considered in order to meet the basic assumption that the residual stress is uniform within each drilling step. The relaxation time between the successive drilling steps was adjusted to 2 min for ensuring the stability of the recorded strain data before conducting the next drilling step. During the drilling process, an air turbine was used to drill the hole with a drilling speed of about 300,000 rpm (3 bar) combined with the orbital technique, which enables the chip to freely move out of the hole, avoiding inducing new stresses in the material. Due to this technique, a hole of sufficiently good quality can be achieved [42]. In [13], a novel formalism for in-depth non-uniform residual stress analysis in orthotropic materials was adopted and a solid element with nine elastic constants in finite element analysis (FEA) was utilized for calculating the calibration coefficients (see [13] for more information). Based on the experimentally determined strain and the calculated calibration coefficients, the residual stresses can be evaluated. A three-dimensional finite element model was used for the determination of the calibration coefficients. The prepreg system

SGL Sigapreg E320 was used for the production of the metal/CFRP hybrids in [10,13]. A micro-alloyed steel (HC340LA) was used as the metal component.

Figure 3b,c depict the calculated residual stresses in the thickness direction for the CFRP and steel components. Due to the diameter of the chosen drill, a reliable prediction by the hole drilling method is limited up to a depth of 0.8 mm [13]. It can be noted, that the numerically predicted and the experimentally determined results are in good agreement. The state of residual stress determined by the simulated incremental HDM also agrees well with the experimental results. It should be noted, that the formulas for calculating the residual stress distribution are based on the assumption of an perfect laminate. Therefore, inherent defects, like the fiber waviness, have not been accounted for.

3. Analysis of Fiber Waviness on the Residual Stress State and the Reliability of the HDM

3.1. Definition of Fiber Waviness

The application of the incremental HDM represents a challenge on the CFRP side due to the heterogeneous microstructure. The influence of process-related defects, such as fiber waviness, on the residual stress state and its prediction using the HDM, is unknown. In this section the influence will be investigated using a simplified representation of a homogeneous fiber waviness. In this context a sinusoidal fiber waviness is assumed in the form

$$a \cdot \sin\left(\frac{2\pi \cdot x}{L}\right) \quad (1)$$

The fiber waviness is determined by the amplitude a and the wavelength L , whereby x describes the position in lateral direction. Accordingly, the angle of slope $\alpha(x)$ can be written as

$$\alpha(x) = \arctan\left(\frac{2\pi \cdot a}{L} \cdot \cos\left(\frac{2\pi \cdot x}{L}\right)\right) \quad (2)$$

Using the user subroutine ORIENT, the slope angle varying along the x-axis is defined as a rotation angle around the z-axis for in-plane waviness and around the y-axis for an out-of-plane waviness (thickness direction). The fiber waviness that occurs for the two considered cases is depicted in Figure 4.

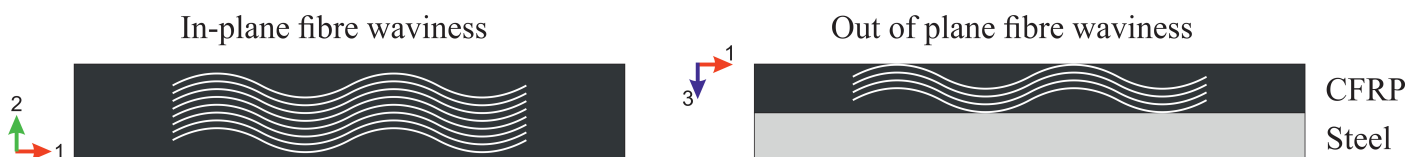


Figure 4. Visualization of the fiber waviness under consideration. Each fiber waviness has been studied independently of each other. Furthermore, the fiber waviness has been assumed to be uniform within the entire cross-section.

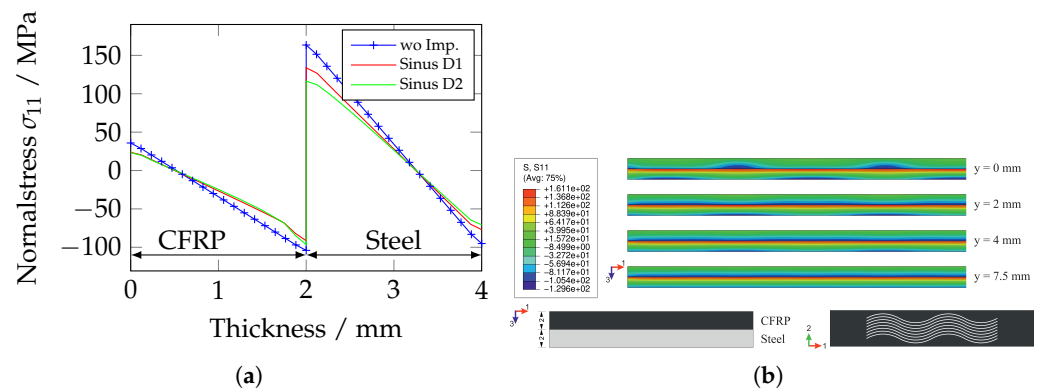
3.2. Analysis Results

3.2.1. In-Plane Fiber Waviness

In Figure 5a, the resulting residual stresses are plotted over the specimen thickness and compared to the unidirectional composite without imperfection. The investigations on fiber waviness have been carried out for two sinus profiles, which differ in amplitude and wavelength (Table 2). The placement of the fiber waviness in the x–y plane results in an overall reduction of residual stresses (Figure 5a). The reduction is particularly evident on the free surface of the CFRP (–45%) and the interface on the metal side (–29%). The influence of the amplitude and wavelength of the fiber waviness is small on the CFRP side, while the deviation at the interface on the metal side is approximately 17 MPa, whereas on the free outer surface of the metal the deviation is reduced to approximately 7 MPa.

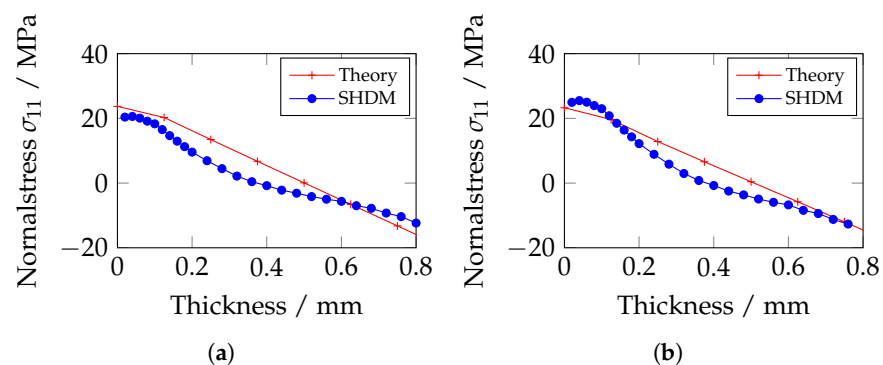
Table 2. Values of wavelength and amplitude for the sine function used for defining fiber waviness (Equation 3.1 [38]).

Label	a [mm]	L [mm]
Sinus D1	0.0526	2.29
Sinus D2	1.19	27.9

**Figure 5.** (a) Residual stress states with an in-plane fiber waviness compared to the reference residual stress state (without any imperfections). (b) Contour plot of the residual stress distribution σ_{11} shown for four section planes. The oscillation of the residual stress in thickness direction decreases rapidly from the boundary ($y = 0$ mm), after 2 mm the oscillation is almost absent.

The scattering of the residual stress distribution in thickness direction is low. Only at the free edges, oscillating residual stresses in the thickness direction can be seen, which rapidly decay as the distance from the edge increases (Figure 5b). The residual stresses in the fiber direction are shown for the sinusoidal profile D2 for three section planes (x - z plane) in Figure 5b, whereby $y = 0$ mm represents the outer surface in x - z plane.

The simulated hole drilling method reveals that the reduced residual stress conditions can still reliably predicted (Figure 6). If the strain fields around the borehole are considered (Figure 7), the anisotropy of the strain field around the borehole is shown to have already decayed by the time the strain gauges are reached. It should be noted, that deviations in the strain measurement in the fiber direction would influence the residual stress measurement more than the transverse strain, which can be explained by the transverse elastic characteristics and the aspect ratio of transverse-to-longitudinal elastic modulus. It should be noted, that the formulas for calculating the residual stress distribution are based on the assumption of an idealized laminate without any inherent defects, as for example the fiber waviness [13].

**Figure 6.** Comparison of the theoretical residual stress and the predicted residual stress state using the simulated hole drilling method for the in-plane waviness. (a) Sinus D1; (b) Sinus D2.

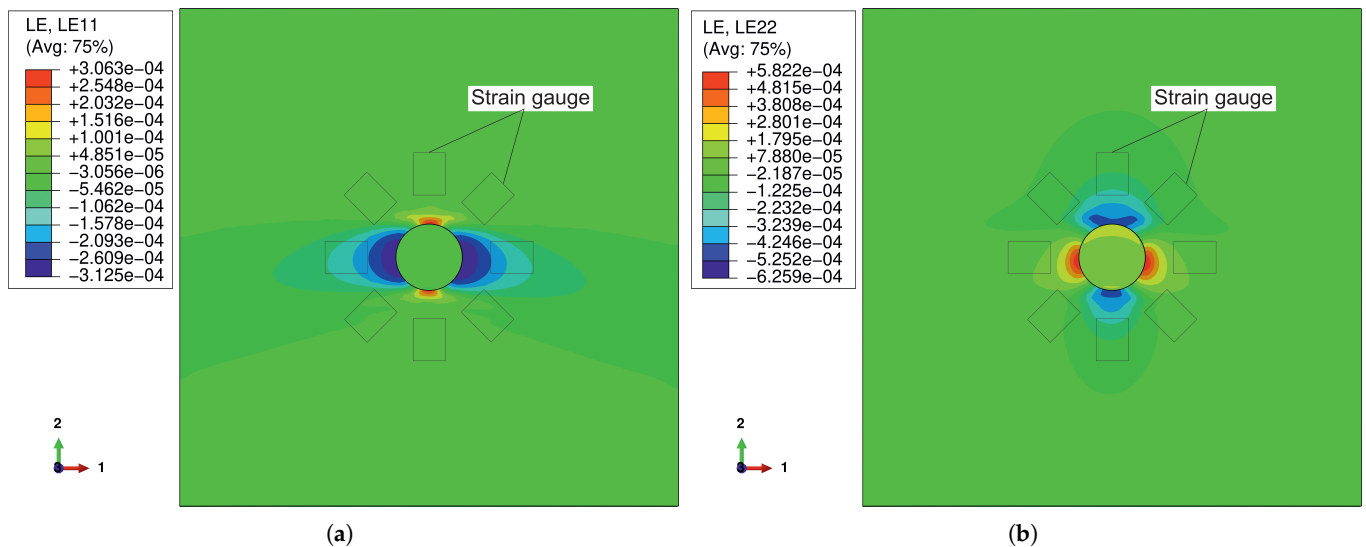


Figure 7. Contour plot of the strain distribution ((a) ϵ_{11} , (b) ϵ_{22}) around the borehole at a drilling depth of 0.8 mm. The placement of the strain gauges is shown in the figures. Due to the (in-plane) fiber waviness, the strain distribution around the borehole is not symmetrical.

3.2.2. Out-of-Plane Fiber Waviness

In the next section, the out-of-plane fiber waviness is analyzed. Figure 8 first presents the residual stress σ_{11} over the section thickness. In contrast to the in-plane fiber waviness, the oscillation of the stress distribution is not limited to the boundary regions, instead it remains constant along the y-axis. The residual stress curves are plotted at three characteristic points (Figure 8).

The variance of the residual stress level at the free surface of the CFRP and metal, as well as at their interface is significantly more pronounced as compared to the results obtained for the in-plane fiber waviness. In the interface, the scattering of stresses is above 115 MPa on the metal side and about 60 MPa on the CFRP side. On the outer metal side the stresses scatter in a range of about 130 MPa. The fiber waviness even results in nonlinear progressions in the CFRP (Figure 8, e.g., “Pos. 3”). The oscillation and variance of the residual stresses at the interface is highly interesting in this context, since the interface is a major weak point in the hybrid laminate and the residual stress level present is relevant to its damage behavior.

The orientation of the fibers with or against the global deflection results in a different shear stiffness (shear stress σ_{13}), which eventually leads to oscillating stress fields. Accordingly, the stress curves follow along the x-axis (Figure 8b; “Pos. 1”, “Pos. 3”) with a period of 2π . For short wavelengths and small amplitudes (“Sine D1”), the effects of fiber waviness in the thickness direction are small in terms of stress variation amplitude (Figure 9).

The oscillation of the stress and deformation fields can be rationalized based on the varying shear stiffness (x–z plane) along the transverse direction. The local fiber orientation, which is formed with a period π opposite or in the direction of the overall deformations (Figure 10), has been identified as the source of the varying shear stiffness. Based on the fundamental beam theories according to Timoshenko and Euler–Bernoulli, the underlying application of both theories can be transferred to beam-shaped FRP structures: In the Bernoulli beam theory shear stresses are neglected due to their small amount, consequently the fiber waviness in the thickness direction is also negligible. On the contrary, according to the theory of Timoshenko, shear deformation, for example due to the geometrical dimensions, cannot be further neglected and fiber waviness in the thickness direction must also be taken into account.

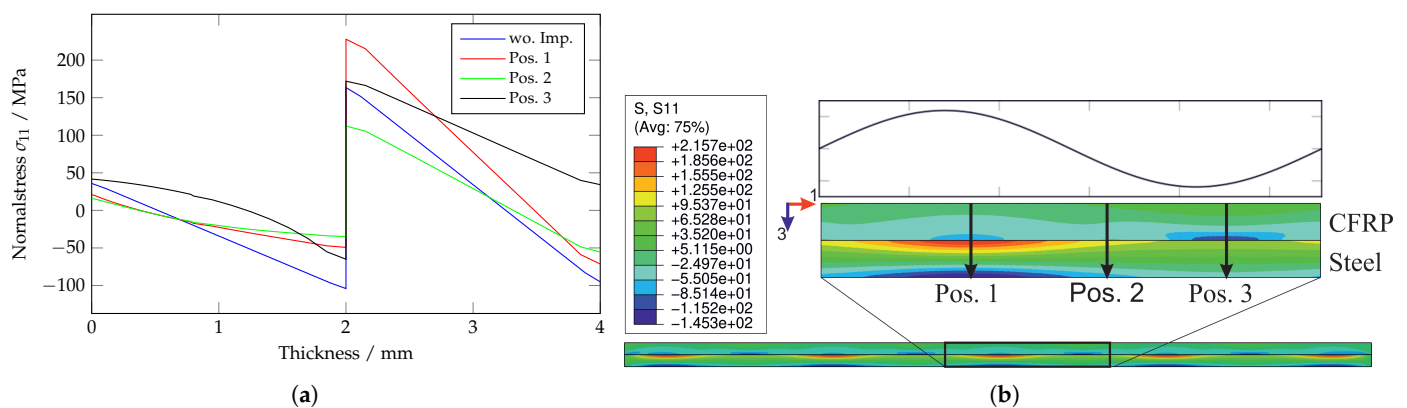


Figure 8. (a) Residual stress states with an out-of-plane fiber waviness (“Sinus D2”) compared to the reference residual stress state. The induced fiber waviness results in oscillating stress and strain fields in thickness direction along the x-axis. In addition, the waviness partially results in non-linear normal stress characteristics (see item 3). (b) shows the normal stresses σ_{11} across the thickness. The corresponding fiber waviness is shown redon top of the enlarged contourplot.

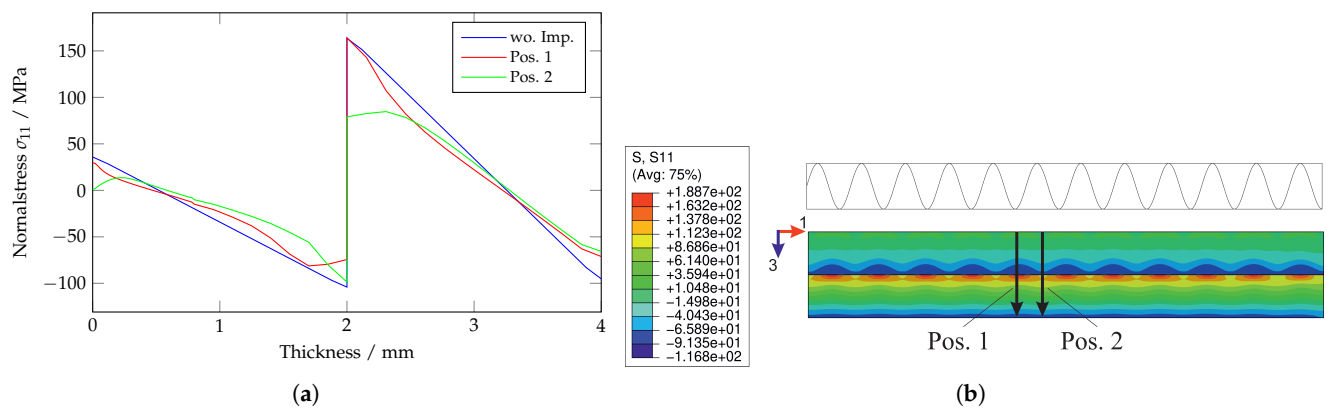


Figure 9. (a) Residual stress states with an out-of-plane fiber waviness (“Sinus D1”) compared to the reference residual stress state. The induced fiber waviness results in oscillating stress and strain fields in thickness direction along the x-axis. (b) The Normal stresses σ_{11} across the thickness. On the top of the enlarged contour plot the corresponding fiber waviness is shown.

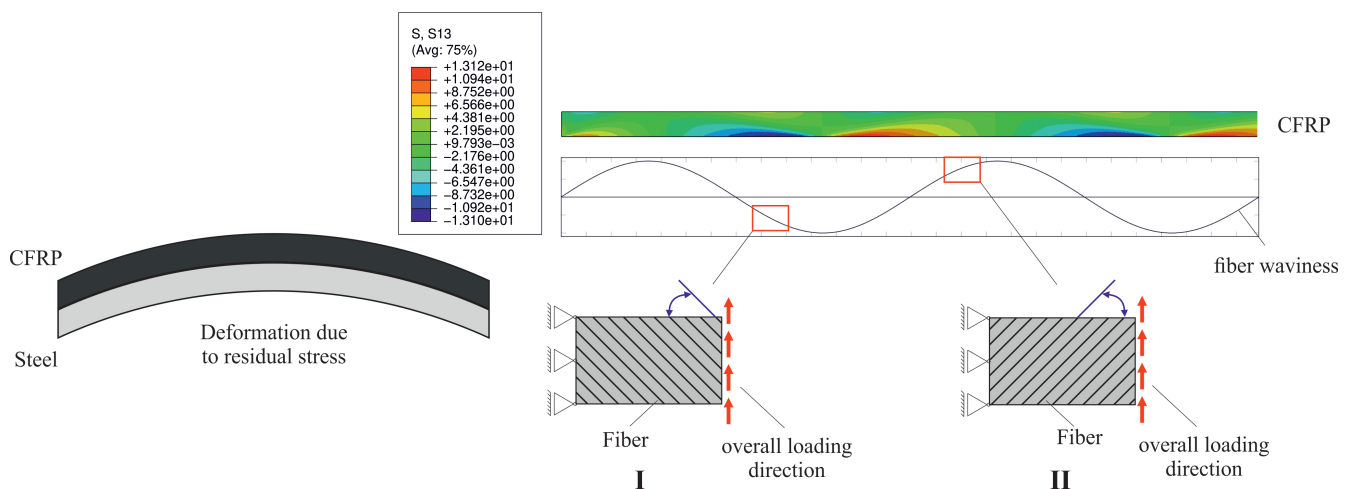


Figure 10. In the contour plot the distribution of the shear stress σ_{13} in the CFRP-section with out-of-plane waviness (sinus D2) is illustrated. Below, the corresponding fiber waviness is plotted accordingly. Maximum shear stresses are located in areas with higher shear stiffness. The varying shear stiffness can be explained by the fact that the fiber orientation can oriented against (I) or with (II) the overall deformation direction.

In present case, the inhomogeneous structure of the FML leads to non-negligible interlaminar shear stresses, which are already present at small cross-sectional dimensions and consequently lead to the observed oscillation.

Up to this point, it can be summarized that the fiber waviness in the thickness direction results in oscillating stress and strain fields, whereas the in-plane fiber waviness only leads to oscillations at the free edges, which, however, rapidly fade away with increasing distance from the edge.

Furthermore, the reliability of the incremental hole drilling method has to be verified in case of out-of-plane fiber waviness. Figure 11 compares the results of the simulated hole drilling method with corresponding fiber waviness (“Sine D2”) and the theoretical residual stress states. The incremental hole drilling method was carried out at the three previously defined characteristic positions (Figure 8). At the first and third position, respectively (“Pos. 1”, “Pos. 3”), the residual stress cannot be determined correctly using the hole drilling method. At position “Pos. 2”, the agreement with the actual residual stress state is better. In Figure 12, the comparison with the small amplitude and wavelength is shown. Again, the simulated hole drilling method cannot yield reliable results (Figure 12b). Even if the agreement at the first position is better, for a reliable measurement the predicted results have to be uniformly exact. In summary, it can be conducted that even the small amplitude-wavelength fiber imperfection leads to a critical variation of residual stresses along the x-axis (Figure 9). The unreliable prediction of the hole drilling method for the presented case can be explained by the fact, that the waviness effect was not accounted for in the calculation of the calibration coefficients.

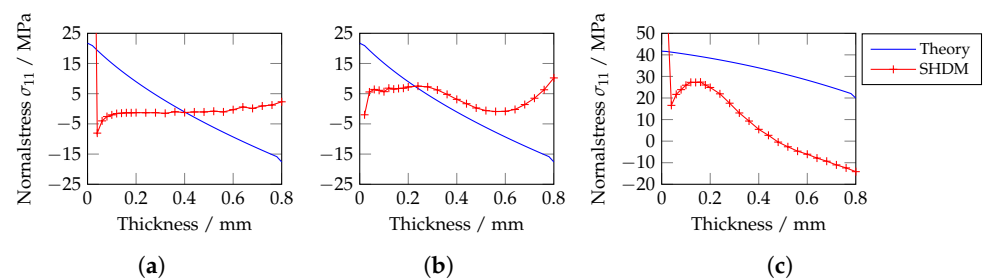


Figure 11. Comparison of the theoretical residual stress and the predicted residual stress state using the simulated hole drilling method for the out-of-plane waviness “Sinus D2”. The comparison is done at the three characteristic positions (Figure 8). It can be clearly observed that the induced fiber imperfection lead to recognizable deviations. (a) Pos. 1; (b) Pos. 2; (c) Pos. 3.

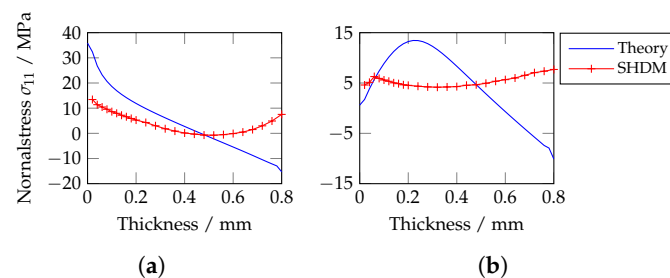


Figure 12. Comparison of the theoretical residual stress and the predicted residual stress state using the simulated hole drilling method for the out-of-plane waviness “Sinus D1”. The comparison is done at the two characteristic positions (Figure 9). It can be clearly observed that the induced fiber imperfection lead to recognizable deviations. (a) Pos. 1; (b) Pos. 2.

4. Conclusions

Fiber waviness is one of the most common defects in composite materials. The production-related defects can be induced by stacking of individual layers, injection of resin or by the pressing process. Fiber waviness cannot be completely avoided, especially in case of geometrically complex components. In this context, it is of high importance

to investigate the influence of the fiber waviness on the overall residual stress state and furthermore the applicability of the incremental hole drilling method. In [40], a reduced effective elastic modulus determined by an extension of the classical laminate theory was presented. However, due to the employed homogenization scheme the oscillating stress fields were neglected and cannot be predicted by this approach. As one can see in the presented study, this is quite important, as the oscillating stress fields have a major influence on the applicability and reliability of the hole drilling method. Moreover, with the presented approach, it is possible to study the resulting oscillating stress fields with respect to the damage initiation at the interphase. The main results can be drawn as follows:

1. In-plane fiber waviness leads to a rather low variance of residual stresses over thickness. Furthermore, oscillation of residual stresses occurs only at the boundaries of the samples section, which, however, quickly fades away. The simulated hole drilling method has proven that the residual stresses along the thickness direction can still be determined precisely in the case of such an in-plane waviness. The results indicated that the residual stress is not sensitive to the wave length and amplitude, if the waviness is in-plane.
2. Out-of-plane fiber waviness is much more critical with regard to the distribution and variance of residual stresses. The oscillation of residual stresses occurs over the entire sample width and is not limited to the boundary layers, as in the case of the in-plane fiber waviness described above. In addition, the investigation of two kinds of sinusoidal fiber waviness indicated that the long-wave profile with higher amplitude leads to significantly higher scattering of residual stresses, especially at the metal-CFRP interface. Applying the simulated hole drilling method, it was shown that the fiber waviness in thickness direction is a challenge for the determination of residual stress states such that the approach could not provide satisfactory results in the form of correct residual stress predictions.
3. Additionally it could be shown that the waviness in loading direction leads to a varying shear stiffness. This can be related to the kinematic of the fiber orientation, which can be with or against the overall loading direction. If shear stresses are present (e.g., in Timoshenko-Theory, multimaterial layup), this kind of fiber waviness leads to the oscillation of deformation fields.
4. The current limits of the incremental hole drilling method could be pointed out by the presented investigations. Without further adjustment of the calibration coefficients the oscillating stress and strain fields lead, in particular fiber waviness in thickness direction, to unreliable predictions. For the experimental application it can be concluded that the specimens have to be carefully examined with regard to fiber waviness, which, however, in most cases will be difficult to determine.

Further investigations of the authors will include analysis of the influence of pores regarding the reliability of the hole drilling method. In this context the numerical approach will be extended. FFT-based homogenization techniques seem to be an promising approach. With respect to the oscillating residual stresses at the interface, the damage initiation of intrinsically manufactured hybrids will be further investigated.

Author Contributions: Conceptualization, S.T.; methodology, S.T.; software, S.T.; validation, S.T. and T.W.; formal analysis, S.T.; investigation, S.T.; resources, T.T. and T.N.; data curation, S.T. and T.W.; writing—original draft preparation, S.T.; writing—review and editing, S.T., T.W., T.T. and T.N.; visualization, S.T.; supervision, T.T. and T.N.; project administration, S.T. and T.W.; funding acquisition, T.T. and T.N. All authors have read and agreed to the published version of the manuscript.

Funding: This research was supported by the Deutsche Forschungsgemeinschaft (DFG) (project number 399304816). The authors gratefully acknowledge for the financial support. The authors gratefully acknowledge the funding of this project by computing time provided by the Paderborn Center for Parallel Computing (PC²).

Institutional Review Board Statement: Not applicable.

Informed Consent Statement: Not applicable.

Data Availability Statement: Data available upon reasonable request.

Conflicts of Interest: The authors declare no conflict of interest.

Abbreviations

The following abbreviations are used in this manuscript:

AHSS	Advanced high strength steels
BIW	Body in white
CFRP	Carbon fiber reinforced plastics
FML	Fiber metal laminates
CTE	Coefficient of thermal expansion
CCS	Coefficient of chemical shrinkage
HDM	Incremental hole drilling method
RVE	Representative volume element
DOC	Degree of cure
FEA	Finite element analysis
SHDM	Simulated hole drilling method
S_{11}, σ_{11}	Normal stress in x direction [MPa]
S_{13}, σ_{13}	Shear stress in x-z [MPa]
C_{ii}	Entry of fourth order linear elasticity tensor [MPa]
α_{ii}	Coefficient of thermal expansion (CTE) [K^{-1}]
β_{ii}	Coefficient of chemical shrinkage (CCS) [-]
α	Angle of slope
a	Amplitude of fiber waviness [mm]
L	Wavelength of fiber waviness [mm]
ORIENT	User subroutine to prescribe an orientation for defining local material directions
USDFLD	User subroutine to define field variables
GLARE	Glass fiber aluminum reinforced epoxy

References

- Reuter, C.; Tröster, T. Crashworthiness and numerical simulation of hybrid aluminium-CFRP tubes under axial impact. *Thin-Walled Struct.* **2017**, *117*, 1–9. [\[CrossRef\]](#)
- Shanmugam, K.; Gadhamshetty, V.; Yadav, P.; Athanassiadis, D.; Tysklind, M.; Upadhyayula, V.K. Advanced High-Strength Steel and Carbon Fiber Reinforced Polymer Composite Body in White for Passenger Cars: Environmental Performance and Sustainable Return on Investment under Different Propulsion Modes. *ACS Sustain. Chem. Eng.* **2019**, *7*, 4951–4963. [\[CrossRef\]](#)
- Wang, Z.; Lauter, C.; Sanitther, B.; Camberg, A. Manufacturing and investigation of steel-CFRP hybrid pillar structures for automotive applications by intrinsic resin transfer moulding technology. *Int. J. Automot. Compos.* **2016**, *2*, 229–243. [\[CrossRef\]](#)
- Sinmazçelik, T.; Avcu, E.; Bora, M.Z.; Çoban, O. A review: Fibre metal laminates, background, bonding types and applied test methods. *Mater. Des.* **2011**, *32*, 3671–3685. [\[CrossRef\]](#)
- Koch, S.F.; Barfuss, D.; Bobbert, M.; Groß, L.; Grützner, R.; Riemer, M.; Stefaniak, D.; Wang, Z. Intrinsic Hybrid Composites for Lightweight Structures: New Process Chain Approaches. *Adv. Mater. Res.* **2016**, *1140*, 239–246. [\[CrossRef\]](#)
- Schimanski, K.; Schumacher, J.; Wottschel, V.; von Hehl, A.; Zoch, H.W.; Vollertsen, F. Characterization of Ti6Al4V for Integral Transition Structures in FRP–Aluminum Compounds. *Steel Res. Int.* **2012**, *83*, 964–971. [\[CrossRef\]](#)
- Parlevliet, P.P.; Bersee, H.E.; Beukers, A. Residual stresses in thermoplastic composites—A study of the literature—Part I: Formation of residual stresses. *Compos. Part A Appl. Sci. Manuf.* **2006**, *37*, 1847–1857. [\[CrossRef\]](#)
- Zahlan, N.; O’Neill, J. Design and fabrication of composite components; the spring-forward phenomenon. *Composites* **1989**, *20*, 77–81. [\[CrossRef\]](#)
- Parlevliet, P.P.; Bersee, H.E.; Beukers, A. Residual stresses in thermoplastic composites—A study of the literature. Part III: Effects of thermal residual stresses. *Compos. Part A Appl. Sci. Manuf.* **2007**, *38*, 1581–1596. [\[CrossRef\]](#)
- Tinkloh, S.; Wu, T.; Niendorf, T. A micromechanical-based finite element simulation of process-induced residual stresses in metal-CFRP-hybrid structures. *Compos. Struct.* **2020**, *238*, 111926. [\[CrossRef\]](#)
- White, S.; Hahn, H. Process Modeling of Composite Materials: Residual Stress Development during Cure. Part I. Model Formulation. *J. Compos. Mater.* **1992**, *26*, 2402–2422. [\[CrossRef\]](#)
- Bogetti, T.A.; Gillespie, J.W.J. Process-Induced Stress and Deformation in Thick-Section Thermoset Composite Laminates. *J. Compos. Mater.* **1992**, *26*, 626–660. [\[CrossRef\]](#)

13. Wu, T.; Tinkloh, S.; Tröster, T.; Zinn, W.; Niendorf, T. Determination and Validation of Residual Stresses in CFRP/Metal Hybrid Components Using the Incremental Hole Drilling Method. *J. Compos. Sci.* **2020**, *4*, 143. [[CrossRef](#)]
14. Zhou, W.; Zhou, H.; Zhang, R.; Pei, Y.; Fang, D. Measuring residual stress and its influence on properties of porous ZrO₂/(ZrO₂+Ni) ceramics. *Mater. Sci. Eng. A* **2015**, *622*, 82–90. [[CrossRef](#)]
15. Guo, J.; Fu, H.; Pan, B.; Kang, R. Recent progress of residual stress measurement methods: A review. *Chin. J. Aeronaut.* **2019**. [[CrossRef](#)]
16. Prussak, R.; Stefaniak, D.; Hühne, C.; Sinapius, M. Evaluation of residual stress development in FRP-metal hybrids using fiber Bragg grating sensors. *Prod. Eng.* **2018**, *12*, 259–267. [[CrossRef](#)]
17. Schajer, G.S.; Yang, L. Residual-stress measurement in orthotropic materials using the hole-drilling method. *Exp. Mech.* **1994**, *34*, 324–333. [[CrossRef](#)]
18. ASTM. *E837-01 Standard Test Method for Determining Residual Stresses by the Hole Drilling Strain-Gage Method*; American Society for Testing and Materials: New York, NY, USA, 2001.
19. Wang, G.D.; Melly, S. Three-dimensional finite element modeling of drilling CFRP composites using Abaqus/CAE: A review. *Int. J. Adv. Manuf. Technol.* **2018**, *94*. [[CrossRef](#)]
20. Phadnis, V.A.; Makhadmeh, F.; Roy, A.; Silberschmidt, V.V. Drilling in carbon/epoxy composites: Experimental investigations and finite element implementation. *Compos. Part A Appl. Sci. Manuf.* **2013**, *47*, 41–51. [[CrossRef](#)]
21. Phadnis, V.A.; Roy, A.; Silberschmidt, V.V. Finite element analysis of drilling in carbon fiber reinforced polymer composites. *J. Phys. Conf. Ser.* **2012**, *382*, 012014. [[CrossRef](#)]
22. Giasin, K.; Ayvar-Soberanis, S.; French, T.; Phadnis, V. Erratum to: 3D Finite Element Modelling of Cutting Forces in Drilling Fibre Metal Laminates and Experimental Hole Quality Analysis. *Appl. Compos. Mater.* **2016**, *24*, 139–140. [[CrossRef](#)]
23. Ameer, M.F.; Zitoun, R.; Habak, M.; Kenane, M. Multi-Scales Analysis of the Damage Induced During One-Shot Drilling of CFRP/Titanium Alloy. In Proceedings of the 18th European Conference on Composite Materials (ECCM-18), Athens, Greece, 25–28 June 2018.
24. Nobre, J.; Stiffel, J.H.; Nau, A.; Outeiro, J.; Batista, A.; Van Paepegem, W.; Scholtes, B. Induced drilling strains in glass fibre reinforced epoxy composites. *CIRP Ann.* **2013**, *62*, 87–90. [[CrossRef](#)]
25. Nobre, J.P.; Stiffel, J.H.; Paepegem, W.V.; Nau, A.; Batista, A.C.; Marques, M.J.; Scholtes, B. Quantifying the Drilling Effect during the Application of Incremental Hole-Drilling Technique in Laminate Composites. *Mater. Sci. Forum* **2011**, *681*, 510–515. [[CrossRef](#)]
26. Aamir, M.; Tolouei-Rad, M.; Giasin, K.; Nosrati, A. Recent advances in drilling of carbon fiber reinforced polymers for aerospace applications: A review. *Int. J. Adv. Manuf. Technol.* **2019**. [[CrossRef](#)]
27. Rohwer, K. Models for Intralaminar Damage and Failure of Fiber Composites - A Review. *Facta Univ. Ser. Mech. Eng.* **2016**, *14*, 1–19. [[CrossRef](#)]
28. Ameen, M.; Peerlings, R.; Geers, M. A quantitative assessment of the scale separation limits of classical and higher-order asymptotic homogenization. *Eur. J. Mech. A Solids* **2018**, *71*, 89–100. [[CrossRef](#)]
29. Zitoun, R.; Krishnaraj, V.; Collombet, F.; Le Roux, S. Experimental and numerical analysis on drilling of carbon fibre reinforced plastic and aluminium stacks. *Compos. Struct.* **2016**, *146*, 148–158. [[CrossRef](#)]
30. Iliescu, D.; Gehin, D.; Iordanoff, I.; Girod, F.; Gutiérrez, M. A discrete element method for the simulation of CFRP cutting. *Compos. Sci. Technol.* **2010**, *70*, 73–80. [[CrossRef](#)]
31. Shokrieh, M.M.; Ghasemi K.A.R. Simulation of Central Hole Drilling Process for Measurement of Residual Stresses in Isotropic, Orthotropic, and Laminated Composite Plates. *J. Compos. Mater.* **2007**, *41*, 435–452. [[CrossRef](#)]
32. Schuster, S.; Steinzig, M.; Gibmeier, J. Incremental Hole Drilling for Residual Stress Analysis of Thin Walled Components with Regard to Plasticity Effects. *Exp. Mech.* **2017**, *57*, 1–11. [[CrossRef](#)]
33. Garnich, M.R.; Karami, G. Localized Fiber Waviness and Implications for Failure in Unidirectional Composites. *J. Compos. Mater.* **2005**, *39*, 1225–1245. [[CrossRef](#)]
34. Kugler, D.; Moon, T.J. Identification of the Most Significant Processing Parameters on the Development of Fiber Waviness in Thin Laminates. *J. Compos. Mater.* **2002**, *36*, 1451–1479. [[CrossRef](#)]
35. Kulkarni, P.; Mali, K.D.; Singh, S. An overview of the formation of fibre waviness and its effect on the mechanical performance of fibre reinforced polymer composites. *Compos. Part A Appl. Sci. Manuf.* **2020**, *137*, 106013. [[CrossRef](#)]
36. Mukhopadhyay, S.; Jones, M.I.; Hallett, S.R. Compressive failure of laminates containing an embedded wrinkle; experimental and numerical study. *Compos. Part A Appl. Sci. Manuf.* **2015**, *73*, 132–142. [[CrossRef](#)]
37. Altmann, A.; Gesell, P.; Drechsler, K. Strength prediction of ply waviness in composite materials considering matrix dominated effects. *Compos. Struct.* **2015**, *127*, 51–59. [[CrossRef](#)]
38. Hsiao, H.; Daniel, I. Effect of fiber waviness on stiffness and strength reduction of unidirectional composites under compressive loading. *Compos. Sci. Technol.* **1996**, *56*, 581–593. [[CrossRef](#)]
39. Karami, G.; Garnich, M. Micromechanical study of thermoelastic behavior of composites with periodic fiber waviness. *Compos. Part B Eng.* **2005**, *36*, 241–248. [[CrossRef](#)]
40. Zhu, J.; Wang, J.; Zu, L. Influence of out-of-plane ply waviness on elastic properties of composite laminates under uniaxial loading. *Compos. Struct.* **2015**, *132*, 440–450. [[CrossRef](#)]

-
41. *Abaqus/CAE User's Manual Version 6.5*; Abaqus: Providence, RI, USA, 2004.
 42. Nau, A.; Scholtes, B. Evaluation of the High-Speed Drilling Technique for the Incremental Hole-Drilling Method. *Exp. Mech.* **2012**, *53*, 531–542. [[CrossRef](#)]